structure. The HRTEM images described here suggest that this structure is also appropriate to the Allende residue carbon.

The HF-HCl residues have been severely processed relative to the original carbon in the meteorite; this processing could have affected the carbon microstructures. For this reason we are now commencing a study of the carbon in situ in the meteorite. Preliminary results indicate the presence of graphitic carbon, similar in appearance to that in the acid residues, occurring interstitially to the silicate grains. This observation is consistent with the results of Green *et al.* (*10*), who reported poorly crystalline graphite located at grain boundaries in Allende. Thus it appears likely that the microstructure of at least some of the carbon is not affected by the HF-HCl treatment.

The well-ordered concentric graphitic particles found in the residue sample etched in fuming HNO_3 (Fig. 3) provide an interesting problem of interpretation, since such grains were not seen in any unetched samples. They are irregularly distributed in the etched material, and so it is difficult to estimate their volume fraction, but they appear to constitute several percent of this sample. If these grains are not created during the HNO_3 etching, then they must also be present, although not observed, in the unetched residues. One possibility is that they occur in the meteorite, and in the HF-HCl residue, as a coating on a phase that is itself destroyed during the HNO_3 etch. The HRTEM studies of the carbon in situ in the meteorite may shed further light on this matter.

If poorly graphitized carbon such as carbonized PVDC is an approximate model for the Allende residue carbon, then it is interesting that such materials have an extremely high gas adsorption capacity (*21*). The specific surface area for nitrogen adsorption in PVDC carbons can be as high as 1400 m^2/g, compared to typical values of < 1 m^2/g for highly graphitized carbons such as those produced from polyvinyl chloride. The Allende residue carbon thus provides a highly plausible site for the retention of the noble gases.

In discussing an adsorption model for the incorporation of noble gases in graphitic carbon, Göbel *et al.* (*22*) showed that it is difficult to account for the high observed gas abundances in meteoritic carbons by using the adsorption parameters for a highly graphitized carbon (specific surface area, 13 m^2/g). This problem is clearly reduced if the specific surface area is two orders of

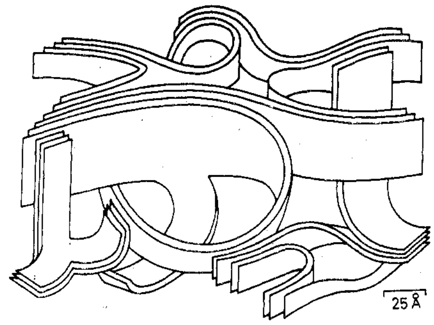

Fig. 4. Schematic diagram of the tangled graphitic structure of the Allende residue carbon, modeled after that of Ban *et al.* (*20*) for carbonized polyvinylidene chloride.

magnitude greater, as seems likely for the Allende carbon. However, simple physical adsorption alone cannot account for the highest release temperatures reported for the noble gases in carbonaceous chondrite acid residues (*5*, *23*); it is necessary to appeal also to a more powerful form of binding, such as solution or occlusion within growing crystallites.

Future evaluation of models for noble-gas retention in carbonaceous chondrite meteorites could be refined by the incorporation of microstructural observations of the kind reported here.

PIERS P. K. SMITH
PETER R. BUSECK

Departments of Geology and Chemistry, Arizona State University, Tempe 85281

References and Notes

1. L. Alaerts and R. S. Lewis, in *Protostars and Planets: Studies of Star Formation and of the Origin of the Solar System*, T. Gehrels, Ed. (Univ. of Arizona Press, Tucson, 1978), p. 439.
2. R. S. Lewis, L. Alaerts, J. I. Matsuda, E. Anders, *Astrophys. J.* **234**, L165 (1979); P. Eberhardt, M. H. A. Jungck, F. O. Meier, F. Niederer, *ibid.*, p. L169.
3. R. S. Lewis, B. Srinivasan, E. Anders, *Science* **190**, 1251 (1975).
4. J. Gros and E. Anders, *Earth Planet. Sci. Lett.* **33**, 401 (1977); R. S. Lewis, L. Alaerts, E. Anders, *Lunar Planet. Sci.* **10**, 725 (1979).
5. J. H. Reynolds, U. Frick, J. M. Neil, D. L. Phinney, *Geochim. Cosmochim. Acta* **42**, 1775 (1978).
6. U. Frick and S. Chang, *Meteoritics* **13**, 465 (1978); U. Ott, *Lunar Planet. Sci.* **11**, 839 (1980).
7. R. S. Lewis, J. Matsuda, A. G. Whittaker, E. J. Watts, E. Anders, *Lunar Planet. Sci.* **11**, 624 (1980).
8. I. A. Breger, P. Zubovic, J. C. Chandler, R. S. Clarke, *Nature (London)* **236**, 155 (1972).
9. J. C. Dran, J. Klossa, M. Maurette, *Lunar Planet. Sci.* **10**, 312 (1979).
10. H. W. Green II, S. V. Radcliffe, A. H. Heuer, *Science* **172**, 936 (1971).
11. A. G. Whittaker, E. J. Watts, R. S. Lewis, E. Anders, *ibid.* **209**, 1512 (1980).
12. R. Hayatsu, R. G. Scott, M. H. Studier, R. S. Lewis, E. Anders, *ibid.*, p. 1515.
13. Six density fractions from an Allende HF-HCl residue were provided by S. Chang of NASA's Ames Research Center. All the results described are from one density fraction (specific gravity < 2.25); no significant differences were observed in the carbon of the other five separates. An analysis of this sample (in percentages), provided by Chang, is as follows: carbon, 60; sulfur, 2.4; chromium, 3.7; iron, 2.6; hydrogen, 1.1; nitrogen, 0.30; nickel and cobalt were present in trace amounts.
14. L. L. Ban, *Surf. Defect Prop. Solids* **1**, 54 (1971).
15. Three samples from a different Allende HF-HCl residue were provided by U. Ott of the University of California, Berkeley; they had been etched for 4 hours in concentrated HNO_3, 17 hours in concentrated HNO_3, and 1 hour in fuming HNO_3, respectively.
16. A. M. Sladkov, V. I. Kasatochkin, Y. P. Kudryavtsev, V. V. Korshak, *Bull. Acad. Sci. U.S.S.R. Div. Chem. Sci.* **1968**, 2560 (1968).
17. V. I. Kasatochkin, V. V. Korshak, Y. P. Kudryavtsev, A. M. Sladkov, V. M. Elizen, *Dokl. Chem.* **214**, 84 (1974).
18. A. G. Whittaker, G. Donnay, K. Lonsdale, *Carnegie Inst. Washington Yearb.* **69**, 311 (1971).
19. R. D. Heidenreich, W. M. Hess, L. L. Ban, *J. Appl. Crystallogr.* **1**, 1 (1968).
20. L. L. Ban, D. Crawford, H. Marsh, *ibid.* **8**, 415 (1975).
21. G. M. Jenkins and K. Kawamura, *Polymeric Carbons* (Cambridge Univ. Press, Cambridge, England, 1976), pp. 137–141.
22. R. Göbel, U. Ott, F. Begemann, *J. Geophys. Res.* **83**, 855 (1978).
23. B. Srinivasan, R. S. Lewis, E. Anders, *Geochim. Cosmochim. Acta* **42**, 183 (1978).
24. We thank S. Chang, U. Ott, and J. H. Reynolds for supplying samples; S. Turner for helpful discussions; and E. Anders, S. Chang, and R. S. Lewis for critical reviews of the manuscript. The electron microscopy was performed in the Facility for High Resolution Electron Microscopy, Arizona State University, established with support from the NSF Regional Instrumentation Facilities Program (grant CHE-7916098). The work was supported by NASA grant NAG 9-4.

14 October 1980; revised 23 December 1980

Evidence of Sea Spray Produced by Bursting Bubbles

Abstract. *Measurements of air bubbles and sea spray are compared, showing that bubble bursting is the major mechanism for producing spray.*

Sea spray affects many natural phenomena and human activities. Meteorologists have related sea salt carried upward by small droplets to the formation of rain (*1*, *2*). Oceanographers have suggested that sea spray plays a major role in transferring heat (*3*), water vapor (*4*), and material (*5*) across the sea surface and viruses (*6*) and bacteria (*7*) from the surface. Icing caused by spray can affect a ship's stability, and the salt damages turbines. In remote sensing with microwave radiation, spray can attenuate backscattering and radiation signals from the sea surface (*8*).

It has been suggested that sea spray is produced through aerodynamic suction at the crests of capillary waves, bursting of air bubbles at the water surface, and direct tearing of crests by the wind. None of these mechanisms has been experimentally verified, although bubble bursting has received the most attention (*9*). In this report, recent measurements of sea spray and air bubbles are reanalyzed, showing that bubble bursting is the major mechanism of spray production, at least under frequently occurring wind velocities.

Droplets produced by bursting bubbles can be in the form of either film drops or jet drops. A film cap develops as an air bubble reaches the water surface and then thins through gravitational drainage and suction caused by the negative curvature of the film boundary (*10–12*). As the bubble breaks, most of the film drops produced move horizontally, the trajectories reaching a few millimeters above the surface. Only a few drops torn off the toroidal rim of the cap are carried upward by the escaping air; most are so small that they stay airborne and evaporate very rapidly (*10, 11*).

The driving force behind jet drops is pressure caused by the surface curvature of the rising bubble (*12*). It has been suggested that sea spray consists mainly of jet drops (*13*). Previous studies of jet drops were conducted in still air (*14–16*). The results reported in (*15*) and (*16*) were summarized by Wu (*13*) and are represented by the shaded area in Fig. 1. In general agreement with the results obtained by Mason (*14*), the radius of jet drops is seen to fall between 10 and 20 percent of that of their parent bubbles.

Air bubbles were measured with a trap by Kolovayev (*17*) in subtropical Atlantic Ocean waters, where the water temperature was uniform to a depth of 25 m and averaged 14°C. A photographic method was used by Johnson and Cooke (*18*) to measure bubble populations and spectra in coastal waters during winter, with the water temperature between 2° and 3°C. Wind velocity was 6 to 13 m/sec in the former investigation and 8 to 13 m/sec in the latter. The distributions of bubble sizes obtained in these investigations were normalized with the total bubble population (*19*) to obtain the probability density functions for the occurrence of bubbles of various sizes as $f = n\Delta R/\Sigma n\Delta R$, where n is the number of bubbles counted within radius band ΔR.

The normalized size spectra of bubbles measured by Kolovayev and by Johnson and Cooke are roughly similar. However, the latter study was conducted in coastal waters, where bubble production may be different from that in open sea. Also, the water temperature was very low. The results of Kolovayev are therefore selected for comparison with Preobrazhenskii's (*20*) measurements of spray, to be discussed later, conducted in open sea with a comparable water temperature. The size spectra of bubbles are seen in Fig. 2 to be invariant with depth or wind velocity.

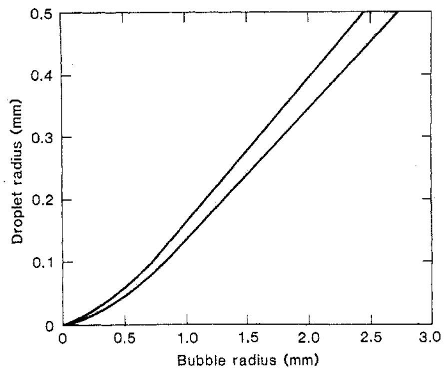

Fig. 1. Water droplets produced by bursting air bubbles.

Preobrazhenskii's measurements of sea spray were made in autumn in the North Atlantic. To collect the droplets, oil-coated plates were attached to a ship's boom and held 1.5 to 2, 4, and 7 m above the sea surface. The data were presented in terms of $p = P/TU$, where P is the number of droplets collected within radius band Δr per unit plate area during exposure time T and U is the wind velocity. Preobrazhenskii's results were grouped according to whether the wind was moderate (7 to 12 m/sec) or strong (15 to 25 m/sec). The velocity range for moderate wind is about the same as that under which Kolovayev (*17*) measured bubbles. Preobrazhenskii's results obtained during moderate winds were normalized by the same procedure discussed earlier to determine probability densities for the occurrence of droplets of various sizes. The normalized distributions of the sizes of droplets collected at various plate elevations are also presented in Fig. 2, and are seen to follow the same trend.

The size spectra of bubbles and droplets, as shown in Fig. 2, are very similar, and approach asymptotically the line of the same slope drawn to approximate bubble and droplet spectra. Furthermore, the drop-off in the droplet size spectra occurs at a size range well within 10 to 20 percent of that for the bubble size spectra. This ratio follows very closely that shown in Fig. 1. In summary, the size spectra of bubbles and drop-

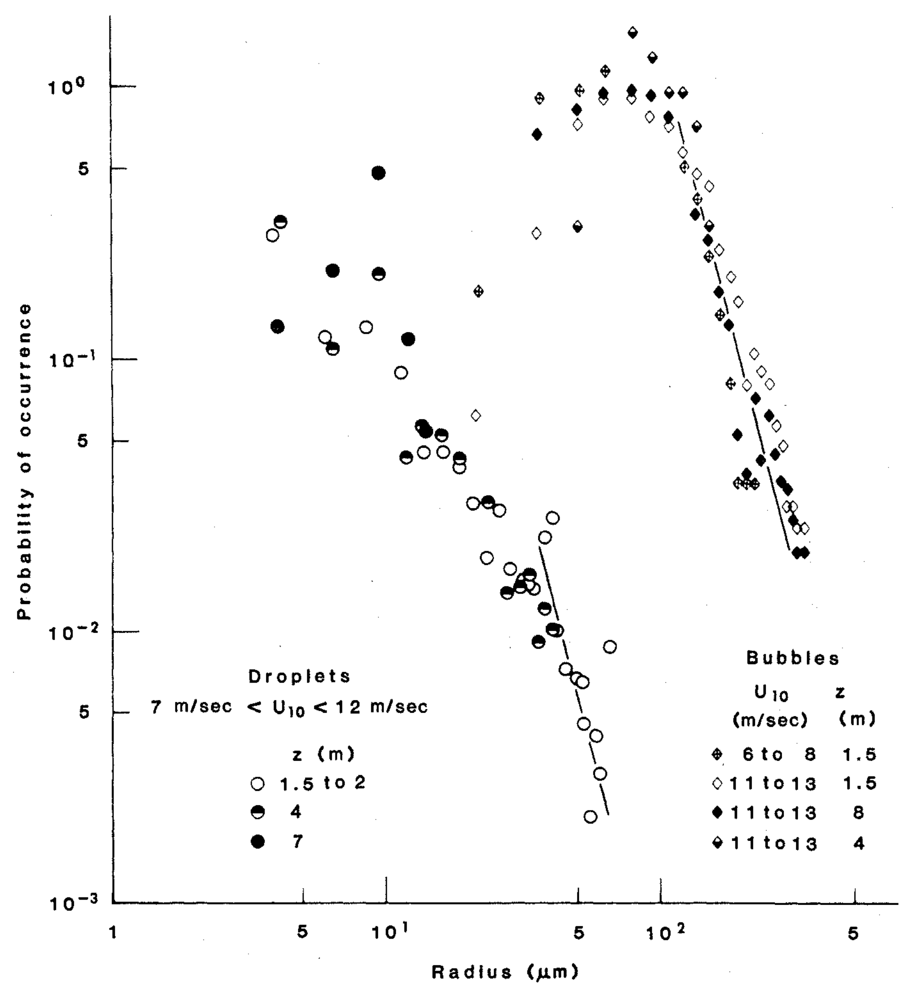

Fig. 2. Size spectra of droplets measured by Preobrazhenskii (*20*) and of bubbles measured by Kolovayev (*17*) (z, elevation of collection plate or depth of data collection; U_{10}, wind velocity at 10 m above sea surface).

lets measured in the open sea are very similar, and the size ratio between bubble and droplet spectra is also very similar to that between jet drops and their parent bubbles. Consequently, sea spray appears to be produced mainly by bubble bursting.

At very low wind velocities, spray may be produced by aerodynamic suction at the crests of capillary waves (no actual observation of this has been reported). Accepting this, the number of droplets produced by aerodynamic suction would still be less than the number produced by bubble bursting because there are 10^5 to 10^6 bubbles per cubic meter for the wind velocity range shown in Fig. 2 and relatively few capillary waves on the wind-disturbed water surface (*19*).

At very high wind velocities, water is torn from the wave crests. However, for a limited wind velocity range the bubble concentration increases very rapidly with wind velocity as $U^{4.5}$ (*19*), and for a wide range of velocities the whitecap coverage also increases very rapidly with wind velocity as $U^{3.75}$ (*21*). In other words, although tearing of the water surface occurs at high wind velocities, the bubble concentration, and therefore the concentration of droplets produced by bursting bubbles, also increases very rapidly. Furthermore, the water torn from the wave crest tends to fall back immediately. Thus, bubble bursting appears to be the major mechanism for spray production even at low and high wind velocities.

It is important to identify clearly the mechanisms of spray production in order to estimate quantitatively the effects of spray, especially atmospheric fluxes of metals and organic matter to and from the ocean and material transport from the sea surface. This report should be helpful in establishing the relative importance of bubbles for transporting sea salts and pollutants to air and land.

JIN WU

College of Marine Studies,
University of Delaware,
Newark 19711

References and Notes

1. A. H. Woodcock, *J. Meterol.* **9**, 200 (1952).
2. ——— and D. C. Blanchard, *Tellus* **7**, 437 (1955).
3. Jin Wu, *J. Geophys. Res.* **78**, 511 (1973).
4. ———, *ibid.* **79**, 4107 (1974).
5. R. A. Duce and E. J. Hoffman, *Annu. Rev. Earth Planet. Sci.* **4**, 187 (1976).
6. E. R. Baylor, M. B. Baylor, D. C. Blanchard, L. D. Syzdek, C. Appel, *Science* **198**, 575 (1977).
7. D. C. Blanchard, *Pure Appl. Geophys.* **116**, 302 (1978).
8. G. R. Valenzuela, M. B. Liang, J. C. Daley, *J. Mar. Res.* **29**, 69 (1971).
9. D. C. Blanchard and A. H. Woodcock, *Ann. N.Y. Acad. Sci.* **338**, 330 (1980).
10. D. C. Blanchard, *Prog. Oceanogr.* **1**, 71 (1963).
11. J. A. Day, *Q. J. R. Meteorol. Soc.* **90**, 72 (1964).
12. F. MacIntyre, *J. Geophys. Res.* **77**, 5211 (1972).
13. Jin Wu, *ibid.* **84**, 1693 (1979).
14. B. J. Mason, *Nature (London)* **174**, 470 (1954).
15. D. C. Blanchard and A. H. Woodcock, *Tellus* **9**, 145 (1957).
16. S. Hayami and Y. Toba, *J. Oceanogr. Soc. Jpn.* **14**, 145 (1958).
17. D. A. Kolovayev, *Oceanology* **15**, 659 (1976).
18. B. D. Johnson and R. C. Cooke, *J. Geophys. Res.* **85**, 3761 (1979).
19. Jin Wu, *ibid.*, in press.
20. J. Yu. Preobrazhenskii, *Fluid Mech. Sov. Res.* **2**, 95 (1973).
21. Jin Wu, *J. Phys. Oceanogr.* **7**, 1064 (1979).
22. Supported by Physical Oceanography Program, National Science Foundation, under grant OCE 77-26508.

3 November 1980; revised 16 January 1981

Threads in the Hagfish Slime Gland Thread Cells: Organization, Biochemical Features, and Length

Abstract. *Scanning electron microscopy in conjunction with cell isolation procedures revealed details of the packing of threads in hagfish slime gland thread cells. Biochemical studies indicate that the thread is largely composed of a protein subunit with a molecular weight of 63,500. Mathematical calculations suggest that the thread may attain lengths of 60 centimeters or more.*

The epidermis and epidermally derived slime glands of hagfishes, perhaps the most primitive living vertebrates, produce copious quantities of mucus (*1*). Hagfish mucus (*2*) and mucus-producing tissues (*3–7*) have been described by various investigators. Although the cells of the epidermis proper contribute some mucus to the total secreted by the hagfish, the bulk of the mucus is formed by cells released from highly specialized slime glands. The encapsulated slime glands (Fig. 1A) are connected to the epidermal surface by a small pore; a single row of pores runs lengthwise along the ventrolateral body wall of each side of the animal. The glands are filled with two types of large secretory cells (Fig. 1, A and B): gland mucous cells and gland thread cells. When these cells are discharged through the pore into the surrounding seawater they break (holocrine secretion). The contents of the broken gland mucous cells interact with seawater to form a thick, clear mucus; the gland thread cells, upon breaking, release long fibrous threads that uncoil and become embedded in the mucus, thus increasing the overall viscosity of the mucus. The gland thread cell appears to be highly specialized (*4–7*), but its internal organization has not been elucidated. We now describe the internal organization of the cell's thread and its biochemical composition and offer a mathematical basis for estimating its length (*8*).

Large quantities of isolated gland thread cells are prepared for scanning electron microscopy by a modification of Ferry's electrical stimulation technique (*4*). Briefly, Pacific hagfish (*Eptatretus stoutii*) anesthetized in MS-222 (ethyl *m*-aminobenzoate methanesulfonate) are removed from seawater, draped over a beaker, and blotted dry. A mild electrical shock administered to the skin adjacent to a slime gland pore causes a localized contraction of skeletal muscle cells that surround the capsule of the slime gland. This contraction squeezes both the gland thread and gland mucous cells through the pore of the slime gland onto the epidermal surface where they are harvested with a spatula and immersed in fixative (3 percent formaldehyde and 3 percent glutaraldehyde in 0.1*M* sodium cacodylate, *p*H 7.3). The gland thread cells, which do not uncoil when handled in this manner, are separated from the gland mucous cells, which break under this condition, by mild centrifugation. The thread cells are then washed, rendered conductive by the osmium-thiohydrocarbazide-osmium technique (*9*), dehydrated, and critical-point dried; alternatively, the washed gland thread cells are dehydrated, critical-point dried, and rendered conductive by sputter-coating. Cells prepared either way look similar when viewed with the scanning electron microscope, and loss of the gland thread cell membrane, as frequently occurs, permits direct visualization of the thread.

A mature gland thread cell (Fig. 1C) is roughly ellipsoidal in shape with one end slightly blunted and the other slightly pointed. At the cell periphery the individual thread strands lie adjacent to one another and appear to form a circumferentially oriented, helically wound cable (Fig. 1, C and D). We refer to this peripheral appearance of the thread as the cabling effect since the thread does not form a true cable. The cabling effect is pronounced at the blunt end and middle portion of the cell but becomes less distinct at the pointed end (Fig. 1, C and D). Since many isolated gland thread cells separate, pull apart, or loosen up during preparation for scanning electron microscopy (Fig. 1, E, F, and G), direct visualization of the packing of the thread

